Inorganic Chemistry

Article

pubs.acs.org/IC

A Comparative Study of $LiCoO_2$ Polymorphs: Structural and Electrochemical Characterization of O2-, O3-, and O4-type Phases

Naoaki Yabuuchi,[†,‡] Yuta Kawamoto,[†] Ryo Hara,[†] Toru Ishigaki,[§] Akinori Hoshikawa,[§] Masao Yonemura,[∥] Takashi Kamiyama,[∥] and Shinichi Komaba*[,†,‡]

[†]Department of Applied Chemistry, Tokyo Univ. of Science, Shinjuku, Tokyo, Japan

[‡]Elements Strategy Initiative for Catalysts and Batteries (ESICB), Kyoto University Katsura, Kyoto, 615-8520, Japan

[§]Frontier Research Center for Applied Nuclear Sciences, Ibaraki University, Tokai, Ibaraki, Japan

[∥]Institute of Materials Structure Science, High Energy Accelerator Research Organization, Tsukuba, Ibaraki, Japan

Supporting Information

ABSTRACT: O4-type $LiCoO_2$ as a third polymorph of $LiCoO_2$ is prepared by an ion-exchange method in aqueous media from OP4-[Li, Na]CoO_2, which has an intergrowth structure of O3-$LiCoO_2$ and P2-$Na_{0.7}CoO_2$. O4-type $LiCoO_2$ is characterized by synchrotron X-ray diffraction, neutron diffraction, and X-ray absorption spectroscopy. Structural characterization reveals that O4-type $LiCoO_2$ has an intergrowth structure of O3- and O2-$LiCoO_2$ with stacking faulted domains. Three $LiCoO_2$ polymorphs are formed from the close-packed CoO_2 layers, which consist of edge-shared CoO_6 octahedra, whereas the oxide-ion stacking is different: cubic in the O3-phase, cubic/hexagonal in the O2-phase, and alternate O3 and O2 in the O4-phase. Structural analysis using the DIFFaX program suggests that the O4-phase consists of approximately 30% of O12-domains, while stacking faults are not evidenced for O2-phase. The results suggest that a nucleation process for Na/Li ion-exchange kinetically dominates a growth process of ideal O4-domains because the presence of CoO_2−Li−CoO_2 blocks as O3-domains could be expected to prevent through-plane interaction of Na layers. Electrochemical behavior and structural transition processes for three $LiCoO_2$ polymorphs are compared in Li cells. A new phase, OT#4-type $Li_{0.5}CoO_2$, is first isolated as an intergrowth phase of O3- and T#2-$Li_{0.5}CoO_2$. However, some deviations from ideal behavior as the O2/O3-intergrowth phase are also noted, presumably because of the existence of stacking faults.

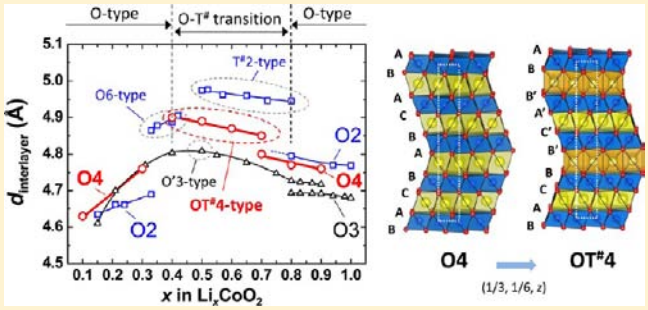

INTRODUCTION

The demand for batteries with a higher energy density has been ever increasing in the past three decades. Rechargeable lithium batteries (so-called Li-ion batteries) have risen to prominence as key devices for green and sustainable energy development. Electric vehicles, which are not equipped with an internal combustion engine, have been launched in the market. Instead of the internal combustion engine, large-scale lithium batteries and electric motors are used as a cleaner and more energy-efficient system. Lithium insertion materials, where lithium ions are topotactically inserted/extracted, are of primary importance to decide the energy density and performance of batteries. As lithium insertion materials, lithium cobalt oxides, $LiCoO_2$, have been substantially studied as positive electrode materials for rechargeable lithium batteries since Sony first commercialized the Li-ion batteries with $LiCoO_2$ in 1991. A research related to the utilization of lithium insertion (intercalation) materials for an electrochemical energy storage technology has started from transition-metal sulfides, such as TiS_2,[1] and layered oxides consisting of high-valence-state transition metals, such as MnO_2,[2] V_2O_5,[3] and MoO_3.[2,3] However, the operating voltage of these electrode materials is limited below 3.5 V vs Li. In 1980, Goodenough's group reported $LiCoO_2$ as a first 4 V class lithium insertion material.[4] Moreover, lithium is incorporated in its framework structure of $LiCoO_2$ in advance, which allows us to design Li-ion batteries with metallic-lithium-free carbon-based materials as negative electrodes. Reaction mechanisms and electrode performance of $LiCoO_2$ have been extensively studied so far.[5−12] A technology of a $LiCoO_2$/graphite cell has become highly sophisticated in the past two decades, and the high-energy Li batteries with $LiCoO_2$ are still widely used as power sources especially for portable electronic devices.

A thermodynamically stable phase of $LiCoO_2$ consists of a cubic close-packed (CCP) oxygen array, in which lithium and cobalt ions are accommodated at distinct octahedral sites because of a size gap between ionic radii of Li^+ (0.74 Å) and Co^{3+} (0.545 Å).[13] $LiCoO_2$ as a thermodynamically stable phase is classified as one of the cation-ordered rocksalt superstructure oxides.[14] Edge-shared LiO_6 and CoO_6 octahedra order into

Received: June 2, 2013
Published: July 17, 2013

   dx.doi.org/10.1021/ic4013922 | Inorg. Chem. 2013, 52, 9131−9142

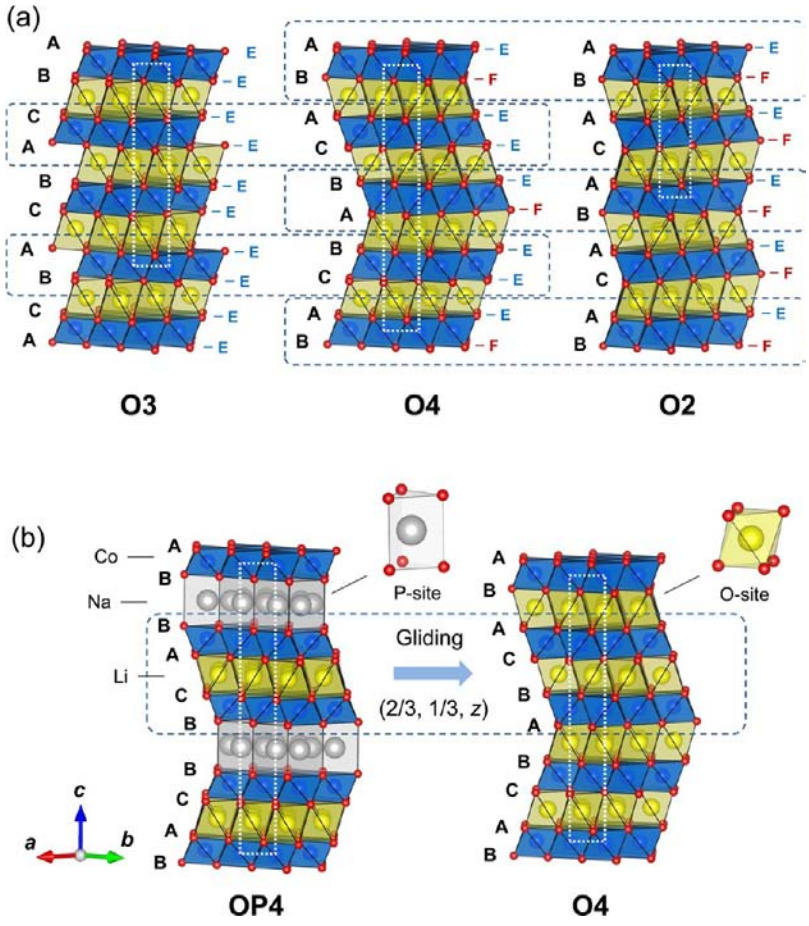

Figure 1. Schematic illustrations of crystal structures for $LiCoO_2$ polymorphs: O2-, O3-, and O4-type $LiCoO_2$ (a). The O4-phase is prepared from OP4-type [Li, Na]CoO_2 by ion-exchange. Half of CoO_2−Li−CoO_2 blocks in the OP4-phase glide toward the direction of (2/3, 1/3, *z*), forming the O4-phase as shown in (b). Na ions are located at trigonal prismatic sites (P-site), whereas Li ions are located at octahedral sites (O-site). After the ion-exchange, Li ions (LiO_6 octahedra) share a face (denoted as "F") with CoO_6 octahedra for one side. In contrast, for the O3-phase (or O3-domains), Li ions (LiO_6 octahedra) only share edges (denoted as "E") with CoO_6 octahedra.

alternate layers perpendicular to [111], forming the LiO_2 and CoO_2 layers, respectively. As a layered structure, $LiCoO_2$ is composed of "*three*" different CoO_2 layers (AB, BC, and CA layers in Figure 1a, left, and a layered stacking manner is crystallographically isostructural with $CdCl_2$) to describe the unit cell, and lithium ions are accommodated at the "*octahedral*" (O) sites between CoO_2 layers. The structure is classified as an O3-type layered structure according to the classification proposed by Delmas et al.[15] The structure is also classified as a 3*R* phase with a space group of $R\bar{3}$m. Following the original publication of $LiCoO_2$ as electrode materials for lithium batteries by Goodenough et al.,[4] a polymorph of $LiCoO_2$ was reported as a metastable phase, which was prepared by an ion-exchange method from a $Na_{0.7}CoO_2$ precursor.[16−19] $Na_{0.7}CoO_2$ is also the layered structure, consisting of "*two*" CoO_2 layers (AB and BA layers). Since the size of sodium ions is much larger than that of lithium ions, the sodium ions are located at trigonal "*prismatic*" (P) sites. The structure is classified as a P2-type layered structure (and also as a 2*H* phase with a space group of $P6_3/mmc$). The $LiCoO_2$ polymorph can be prepared from the P2-type phase by the ion-exchange process without breaking Co−O bonds. Lithium ions, however, cannot be stabilized at the large prismatic sites, resulting in the gliding of CoO_2 layers to form octahedral sites. The CoO_2 gliding leads to the formation of the $LiCoO_2$ polymorph with a unique oxygen packing, AB AC AB AC (Figure 1a, right). In this polymorph, $LiCoO_2$ consists of two CoO_2 layers with AB and AC oxygen arrangements, that is, the O2-type structure. Both O3- and O2-type phases have close-packed oxygen arrays. In the O3-type phase with the CCP array, LiO_2 layers share only edges with CoO_2 layers on both sides. In contrast, the O2-type phase is locally composed of ABA-type and ACA-type (Figure 1a, right) oxygen arrangements, namely, a hexagonal close-packed (HCP) oxygen array. LiO_2 layers, therefore, share faces with CoO_2 layers on the one side. On the basis of oxygen packing, the O2-type structure is classified as an intergrowth structure between CCP and HCP arrays.

The high structural versatility of cobalt oxides as a layered system with alkali-metal ions even results in the formation of a unique lithium-sodium-cobalt ternary layered compound. In 1994, Balsys and Davis reported that $Li_{0.43}Na_{0.36}CoO_{1.96}$ was crystallized into a layered intergrowth structure between O3-$LiCoO_2$ and P2-$Na_{0.7}CoO_2$.[20] Since [Li, Na]CoO_2 has the intergrowth structure, the unit cell of [Li, Na]CoO_2 consists of "*four*" CoO_2 layers. The sample has ordered alternate Li (octahedral sites) and Na (prismatic sites) layers, along the *c*-axis direction, which is classified as the OP4-type phase, as shown in Figure 1b, left. Recently, the existence of a new lithium-sodium-cobalt ternary oxide, OPP9-type phase [Li, Na, Na]CoO_2, was evidenced by Berthelot and coauthors,[21] even

dx.doi.org/10.1021/ic4013922 | *Inorg. Chem.* 2013, 52, 9131−9142

though the authors did not succeed in isolating the OPP sample as a single phase. Since the OP4 and OPP9 phases are intergrowth structures with different oxygen packing as layered materials, the samples have the unique oxygen arrangements. Therefore, similar to the P2-type $Na_{0.7}CoO_2$ phase, these samples can be utilized as precursors for the preparation of $LiCoO_2$ polymorphs. In 2009, our group reported a third polymorph of $LiCoO_2$ prepared from OP4-type [Li, Na]CoO_2 by Na/Li ion-exchange (Figure 1a, center, and Figure 1b, right).[22] Although the Na/Li ion-exchange results in the gliding of CoO_2 layers similar to the O2-phase, its oxygen packing is definitely different from that of the O3- and O2-$LiCoO_2$, as compared in Figure 1a. This polymorph consists of four different CoO_2 layers, and is, therefore, classified as O4-type Li_xCoO_2. Similar to the structural relation for the OP4-type phase, O4-type $LiCoO_2$ is ideally classified as an intergrowth structure between O3- and O2-$LiCoO_2$. Three quarters of lithium layers share edges with CoO_2 layers, and the rest of the layers share faces. The formation of O4-type $LiCoO_2$ from the OP4-phase was also experimentally supported by Berthelot and co-workers.[23]

In this Article, we provide detailed studies of the crystal structures of O4-type Li_xCoO_2 by synchrotron X-ray and neutron diffractions, including an analysis of potential stacking faults based on the O4-type stacking induced by Na/Li ion-exchange from the OP4-type precursor. In addition, comparative studies on three "layered" polymorphs, O2-, O3-, and O4-phases, are provided in relation to local structures around Li ions and phase transition behavior during Li-extraction processes. Although the difference is only the lithium-ion environment associated with stacking sequences of CoO_2 layers, it results in a clear difference in the electrochemical potential based on the reversible Co^{3+}/Co^{4+} redox accompanied with Li extraction, which are easily distinct from each other. From these results, we will discuss the similarities and differences among three polymorphs of layered $LiCoO_2$ as positive electrode materials for rechargeable lithium batteries.

EXPERIMENTAL SECTION

Synthesis of OP4-[Li, Na]CoO_2 and O4-Li_xCoO_2. OP4-[Li, Na]CoO_2 was prepared by a solid-state method from Li_2CO_3 (Kanto Chem. Co., Ltd.; purity, 99%), Na_2CO_3 (Kanto Chem. Co., Ltd.; purity, 99.5%), and Co_3O_4. Co_3O_4 was prepared from $Co(NO_3)_2 \cdot 6H_2O$ (Kishida Chem. Corp.; purity, >98%) by heating at 450 °C for 12 h. A mixture of Li_2CO_3, Na_2CO_3, and Co_3O_4 was pressed into pellets. The pellets were heated in air at 700−1050 °C at a rate of 15 °C min^{-1}, and then the temperature was held at each temperature for 72 h. See the text for more details about the synthesis process of OP4-[Li, Na]CoO_2 samples. The well-characterized OP4-[Li, Na]CoO_2 sample was hydrothermally treated with an aqueous solution of LiOH (2.5 mol dm^{-3}) and LiCl (2.5 mol dm^{-3}) for 24 h using a Teflon-lined autoclave to exchange sodium ions with lithium ions. The chemical composition of Li, Na, and Co was determined by ICP analysis after dissolving the samples in HCl solutions.

For a comparison, O2- and O3-$LiCoO_2$ were also prepared. O3-$LiCoO_2$ was also prepared from Li_2CO_3 and Co_3O_4 at 850 °C for 12 h in air. O2-$LiCoO_2$ was prepared by ion-exchange of P2-$Na_{0.7}CoO_2$, which was prepared by the solid-state method from Na_2CO_3 and Co_3O_4 heated at 800 °C for 48 h in oxygen.

Materials Characterization. Crystal structures of the samples were examined by using an XRD diffractometer (MultiFlex, Rigaku Co., Ltd.) equipped with a graphite monochromator. Cu Kα radiation is utilized as an X-ray source. The samples were covered with a laboratory made attachment during the data collection to avoid air exposure.

Synchrotron X-ray diffraction patterns of the samples were also collected at beamline BL02B2, SPring-8 in Japan, equipped with a large Debye−Scherrer camera.[24] To minimize the effect of X-ray absorption by the samples, the wavelength of the incident X-ray beam was set to 0.5 Å using a silicon monochromator, which was calibrated to 0.5011(2) Å with a CeO_2 standard. Structural analysis by the Rietveld method was carried out using RIETAN-FP.[25] A simulation of stacking faults of the samples was performed with the DIFFaX program.[26] See the text for detailed conditions for the simulation.

The time-of-flight neutron diffraction (TOFND) experiment was conducted at iMATERIA,[27] BL20 of Materials and Life Science Experimental Facility (MLF), J-PARC, in Japan. The sample was sealed in vanadium tubes (6.0 mm in diameter) in an inert atmosphere. The TOF-ND data were collected using a high-resolution bank ($\Delta d/d$ = 0.16%), which covers the d-range of 0.18 < d (Å) < 5. TOFND data were collected at room temperature.

X-ray absorption spectroscopy (XAS) was conducted at BL-7C of the Photon Factory Synchrotron Source in Japan. XAS spectra were collected with a silicon monochromator in a transmission mode. The intensity of incident and transmitted X-rays was measured using an ionization chamber at room temperature. The sample was sealed in a water-resistant polymer film in the Ar-filled glovebox, and then XAS spectra were collected with the minimized damage by moisture. Analysis of the XAS spectra was carried out using the program code IFEFFIT.[28] The postedge background was determined using a cubic spline procedure. Following the subtraction of the background, the XAS spectra were normalized to compare the data with reference samples.

Coin-type cells (R2032-type) were assembled to evaluate the electrode performance of three different $LiCoO_2$ polymorphs. Positive electrodes consisted of 80 wt % active materials, 10 wt % acetylene black, and 10 wt % poly(vinylidene fluoride), which were mixed with *N*-methylpyrrolidone and pasted on Al foil, and then dried at 80 °C in vacuum. Metallic lithium foil was used as a negative electrode. Electrolyte solution used was 1.0 mol dm^{-3} $LiPF_6$ dissolved in ethylene carbonate and dimethyl carbonate; EC/DMC = 1:1 by volume (Kishida Chem. Co., Ltd.). A microporous polyolefin membrane was used as a separator.

RESULTS AND DISCUSSION

Synthesis of OP4-[Li, Na]CoO_2. First, an optimized synthesis condition of OP4-[Li, Na]CoO_2 is explored to prepare phase-pure O4-type $LiCoO_2$ polymorph. Recently, the lithium-sodium-cobalt ternary oxide system was revisited by Berthelot and coauthors, and the authors reported the complicated behavior in relation to phase segregation among four different phases, O3-$LiCoO_2$, P2-$NaCoO_2$, OP4-[Li, Na]CoO_2, and OPP9-[Li, Na, Na]CoO_2.[21] Phase-pure OP4-$Li_{0.42}Na_{\sim 0.41}CoO_2$ was prepared using a complicated synthesis protocol from a mixture of O3-$LiCoO_2$ and P2-$Na_{0.7}CoO_2$, which was tightly sealed in a gold tube.[21] Synthesis from O3-$LiCoO_2$ and P2-$Na_{0.7}CoO_2$ is also utilized by Balsys and Davis.[20] In our Article, we have tuned a simple protocol based on the direct synthesis from sodium and lithium carbonate with cobalt oxides, following the report by Ren et al.[29] Figure 2 compares X-ray diffraction patterns of the lithium-sodium-cobalt ternary oxide with different synthesis conditions. A molar ratio in the precursor was fixed to be Li/Na/Co = 0.43:0.39:1.00 that was decided based on the results of our optimization process. When the sample is synthesized at 700 °C, two phases are found in an X-ray diffraction (XRD) pattern. Phase analysis on the XRD pattern clearly evidenced that the sample is a mixture of two layered phases, that is, O3-type $LiCoO_2$ and P2-type Na_xCoO_2. The OP4 phase appears when the synthesis temperature increases to ∼850 °C. However, when the sample is relatively slowly cooled to room

dx.doi.org/10.1021/ic4013922 | Inorg. Chem. 2013, 52, 9131−9142

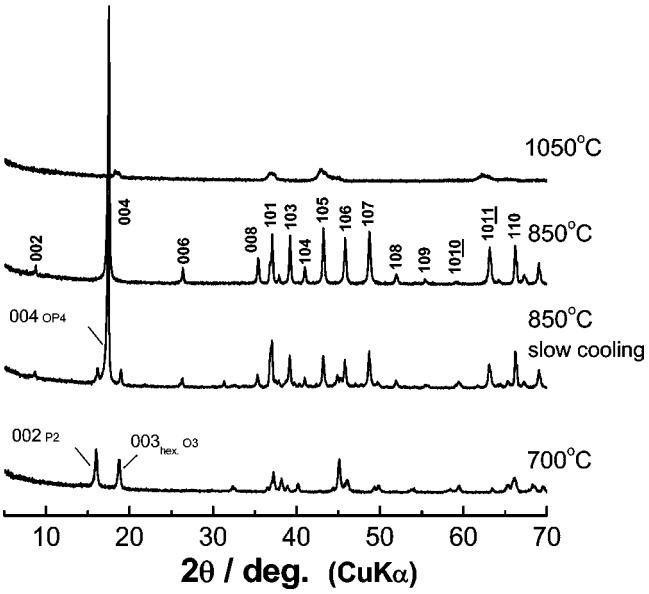

Figure 2. X-ray diffraction patterns of OP4-[Li, Na]CoO_2 samples that were heated with different experimental conditions. See the text for more details.

temperature from 850 °C, for instance, at a cooling rate of 15 °C min^{-1}, three phases are found in an XRD pattern. The major phase can be assigned to the OP4-phase with O3-$LiCoO_2$ and P2-Na_xCoO_2 as two minor phases. In contrast, a single phase of OP4-phase is successfully obtained using a fast cooling process. The pellet was taken out from the furnace at 850 °C without the cooling process after heating for 72 h in air, and then immediately transferred into an Ar-filled glovebox to cool the pellet down fast. The sample was cooled down to room temperature and kept inside the glovebox without exposure to moist air. The presence of diffraction lines, 002 at 8.8° and 006 at 26.3°, is direct evidence of alternate ordering between Li and Na layers along the *c*-axis direction as the intergrowth structure. These facts indicate that the OP4-phase is a high-temperature phase and segregation into O3-$LiCoO_2$ and P2-Na_xCoO_2 cannot be avoided during the relatively slow cooling process. These observations are essentially consistent with the results found by an in situ high-temperature XRD study,[21] even though clear evidence of OPP9-phase formation was not found in this experimental condition. When the heating temperature rises to ∼1050 °C, a clear change is noted in the XRD pattern. Observed Bragg diffraction lines are assigned into a disordered rocksalt phase at 1050 °C, even though the peak profile is relatively broad. It is speculated that major parts of lithium, sodium, and cobalt ions (Co^{3+}/Co^{2+}) are randomly/uniformly distributed over the octahedral cation sites (the existence of a weak diffraction line located at 18.5° suggests that partial long-range ordering still exists as the ordered rocksalt structure). From these results, in this study, it is decided that OP4-type [Li, Na]CoO_2 should be prepared at 850 °C with the fast-cooling process, and used as a precursor for preparation of O4-type $LiCoO_2$ by an ion-exchange method.

Structural Analysis of OP4-type [Li, Na]CoO_2 by SXRD and TOFND. In the previous section, the phase-pure OP4-type [Li, Na]CoO_2 was successfully synthesized with the simple protocol. In this section, a structural analysis is conducted by a synchrotron XRD (SXRD) method combined with a time-of-flight neutron diffraction (TOFND) method. OP4-[Li, Na]-CoO_2 is known as an off-stoichiometric sample, and its chemical composition is clearly deviated from an ideal intergrowth composition between O3-$LiCoO_2$ and P2-$Na_{0.7}$-CoO_2 as, suggested by Berthelot et al.[21] Therefore, the chemical composition of OP4-[Li, Na]CoO_2 was determined by an inductively coupled plasma method. Chemical composition was decided to be $Li_{0.37}Na_{0.31}CoO_2$ without the assumption of oxygen vacancy formation. Li and Na ion contents are clearly smaller than those of the ideal intergrowth structure, OP4-$Li_{0.5}Na_{0.35}CoO_2$. Although our synthesis methodology from sodium and lithium carbonates with cobalt oxide is the same with the previous report by Ren et al., the chemical composition is clearly different.[29] Ren et al. reported that the sample crystallized into a nearly stoichiometric phase as the ideal composition, $Li_{0.48}Na_{0.35}CoO_2$.[29] In our preliminary examinations, when the high-Li content of 0.48 was utilized as the starting material, O3-$LiCoO_2$ as a minor phase was always observed with OP4-[Li, Na]CoO_2 as a major phase. The phase-pure sample was successfully prepared only with a Li-deficient condition.

Figure 3 compares SXRD and TOFND patterns of OP4-$Li_{0.37}Na_{0.31}CoO_2$. Although the SXRD data were collected from

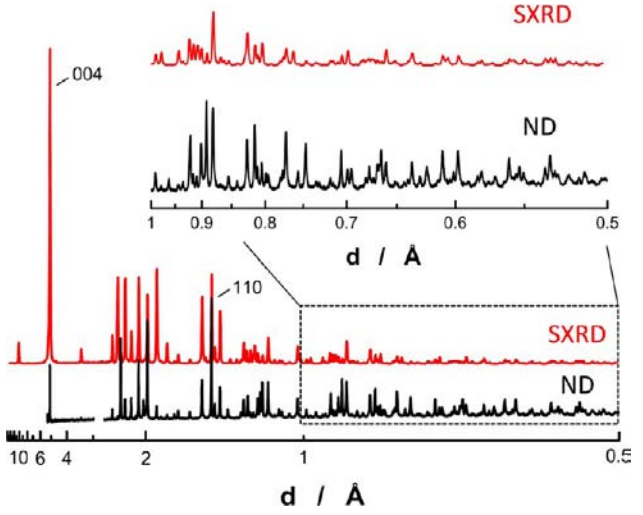

Figure 3. Synchrotron X-ray diffraction (SXRD) and neutron diffraction (ND) patterns of OP4-$Li_{0.37}Na_{0.31}CoO_2$.

a few milligram samples, the diffraction data with an extremely high S/N ratio were obtained within several minutes. The full width at half-maximum (fwhm) of ND data is fairly narrower than that of SXRD because a high-resolution bank ($\Delta d/d$ = 0.16%) was utilized. For instance, the fwhm of the 110 line at d = 1.4 Å is measured to be d = 0.008 and 0.004 Å for SXRD and TOFND, respectively. In addition, the intensity of ND patterns in a shorter d-spacing region (d < 1.0 Å) is much higher than that of SXRD, as shown in Figure 3, inset. For the SXRD pattern, the peak intensity decreases as the d-values decrease. The Rietveld analysis was, therefore, conducted on the SXRD pattern, and the refined data were further validated with the analysis of the TOFND pattern. A result of Rietveld refinement on the SXRD pattern is shown in Figure S1 (Supporting Information), and refined crystallographic parameters are summarized in Table 1. Lattice parameters are calculated to be a = 2.8208(2) Å and c = 20.277(1) Å, which are slightly smaller than the values in the literature.[20,21] The facts are also consistent with the difference in the chemical compositions of

dx.doi.org/10.1021/ic4013922 | Inorg. Chem. 2013, 52, 9131−9142

Table 1. Crystallographic Parameters Refined by the Rietveld Method on a Synchrotron X-ray Diffraction Pattern of OP4-$Li_{0.37}Na_{0.31}CoO_2$[a]

OP4-$Li_{0.37}Na_{0.31}CoO_2$[b]						
atom	site	g	x	y	z	B (Å^2)
Co	4f	1.0	2/3	1/3	0.3843(1)	0.2
Li	2a	0.74	0	0	1/2	0.5
Na (1)	2c	0.39(1)	1/3	2/3	1/4	1.3(1)
Na (2)	2d	0.23(1)	2/3	1/3	1/4	1.2(1)
O (1)	4e	1.0	0	0	0.3364(4)	0.6
O (2)	4f	1.0	1/3	2/3	0.4367(4)	0.6

[a]The data without e.s.d. were fixed and not refined. [b]S.G.: $P6_3/mmc$; a = 2.8208(2) Å and c = 20.277(1) Å. R_{wp} = 10.46% and R_B = 6.12%.

the samples. The sample prepared in this study has slightly less lithium and sodium contents compared with the literature, resulting in the shrinkage of the lattice because of fewer amounts of large sodium ions in the crystal lattice and the oxidation of cobalt for charge compensation. As shown in Table 1, Li and Na ions are located at distinct sites at 2a octahedral and prismatic sites, respectively. Prismatic sites are further separated into two sites: 2c edge-shared and 2d face-shared sites with CoO_6 octahedra. Two prismatic sites with different environments for P2-type Na_xCoO_2 result in the complex nature of Na ion in-plane distributions depending on the Na contents.[30] Since an atomic X-ray scattering factor of Na is large enough, the sodium distribution at the two different prismatic sites was refined in $Li_{0.37}Na_{0.31}CoO_2$. The structural analysis reveals that sodium ions are found not only at edge-shared sites but also at face-shared sites. The occupation was refined to be 39% at edge-shared and 23% at face-shared sites. In addition, relatively large isotropic displacement parameters (1.2−1.3 Å^2) at the prismatic sites are found. This trend is similar to that of P2-$Na_{0.63}CoO_2$[30] and other P2-[31] and OP4-phases.[20,21] According to the literature, the large isotropic displacement parameters were explained by the repulsive interaction with face-shared cobalt.[30] On the basis of the result obtained by Rietveld refinement of the SXRD pattern, occupation of lithium ions, which is almost transparent for X-rays, and isotropic displacement parameters were validated using the ND pattern. The occupation of lithium estimated from the ND pattern is consistent with the result of chemical analysis, and the existence of oxygen vacancies was not evidenced. It is concluded that refined results by SXRD are reasonable as the structural model of $Li_{0.37}Na_{0.31}CoO_2$.

Preparation of O4-type Li_xCoO_2 from OP4-type $Li_{0.37}Na_{0.31}CoO_2$. Na/Li ion-exchange for OP4-$Li_{0.37}Na_{0.31}CoO_2$ was successfully accomplished under a hydrothermal condition.[22] The chemical composition analysis revealed x = 0.9 in Li_xCoO_2 with a trace of sodium in the ion-exchanged sample. An increase in alkali metal ion contents from 0.68 to 0.90 after the ion-exchange process suggests partial reduction of cobalt ions during the hydrothermal treatment. Figure 4 compares SXRD and TOFND patterns of OP4-$Li_{0.37}Na_{0.31}CoO_2$ before and after ion-exchange. The diffraction pattern is completely changed by ion-exchange, as shown in Figure 4. For the SXRD pattern, a clear peak shift for the (004) diffraction line to a higher diffraction angle is observed, indicating that the interlayer (interslab) distance is significantly reduced. The average interlayer distance decreases from 5.07 to 4.72 Å by ion-exchange. This fact is related to that the gliding of CoO_2 layers by Na/Li ion-exchange reduces the electrostatic repulsive

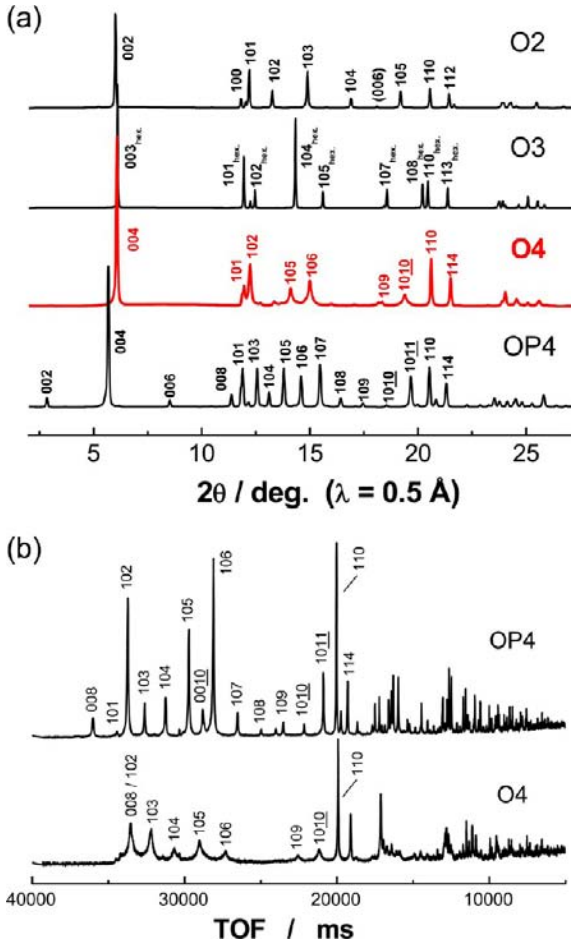

Figure 4. (a) Comparison of SXRD patterns of $LiCoO_2$ polymorphs with the OP4-phase precursor. ND patterns of OP4- and O4-phases are also compared in (b). Peak broadening for 10l diffraction lines of the O4-phase is observed for both SXRD and ND patterns.

force between CoO_2 layers. In addition, 002 and 006 diffraction lines for the OP4-phase disappear by ion-exchange, because Na/Li ion-exchange reduces the electron contrast between two distinct layers. The observed SXRD patterns were further compared with a simulated pattern (Figure S2, Supporting Information), in which it was assumed that one out of two CoO_2−Li−CoO_2 blocks (O3-domains) glided toward the direction of (2/3, 1/3, z) to form the octahedral sites as shown in Figure 1b. Positions of diffraction angles for all of the Bragg diffraction lines agreed well between simulated and experimental patterns in Figure S2 (Supporting Information) and our previous report.[22] Moreover, the diffraction patterns are completely different from those of O2- and O3-phases, as shown in Figure 4a. From these experimental evidence, it is concluded that O4-$Li_{0.9}CoO_2$ (hereafter denoted as O4-$LiCoO_2$ for simplicity) as the third polymorph of $LiCoO_2$ is successfully prepared by the ion-exchange from the OP4-type precursor.

Comparison of Crystal Structures for $LiCoO_2$ Polymorphs. An ideal structural model of O4-$LiCoO_2$ with space group $P6_3mc$ is shown in Table 2. Crystallographic parameters of three different $LiCoO_2$ polymorphs are summarized in Table 3. Although the three samples are polymorphs, the structures are essentially the same as layered materials consisting of stacked CoO_2 layers. Therefore, the in-plane Co−Co distances

dx.doi.org/10.1021/ic4013922 | Inorg. Chem. 2013, 52, 9131−9142

Table 2. Crystallographic Parameters of O4-$LiCoO_2$[a]

O4-$Li_{0.9}CoO_2$[b]					
atom	site	g	x	y	z
Co (1)	2a	1.00	0	0	0
Co (2)	2b	1.00	2/3	1/3	0.248
Li (1)	2b	0.90	1/3	2/3	0.124
Li (2)	2a	0.90	0	0	0.374
O (1)	2b	1.00	2/3	1/3	0.054
O (2)	2a	1.00	0	0	0.194
O (3)	2b	1.00	1/3	2/3	0.302
O (4)	2b	1.00	2/3	1/3	0.446

[a]These parameters, except lattice parameters, were not refined because of the presence of stacking faults. [b]S.G.: $P6^3mc$. a = 2.813 Å and c = 18.86 Å.

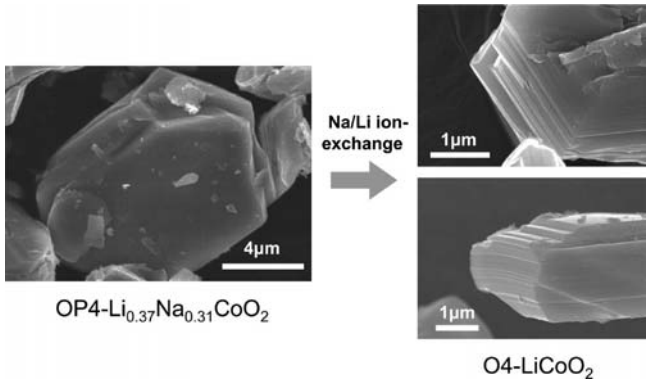

Figure 5. SEM images of OP4-$Li_{0.37}Na_{0.31}CoO_2$, and O4-phase prepared by Na/Li ion-exchange from OP4-$Li_{0.37}Na_{0.31}CoO_2$. The stepped surface morphology is a characteristic feature of the O4-phase.

are almost the same in each sample. The major difference in the crystallographic parameters is found in the interlayer distance. For the O3-phase, Li ions are located at edge-shared octahedral sites with cobalt, whereas for the O2-phase, Li ions are located at face- and edge-shared octahedral sites with cobalt, as shown in Figure 1a. The interlayer distance, therefore, expands by the electrostatic repulsive interaction between Li and Co.[19] Since the O4-phase is classified as an intergrowth structure of O3- and O2-phases, the interlayer distance is also intermediate between two polymorphs. In the O4-type $LiCoO_2$, Li ions are located at two distinct octahedral sites with different local environments at 2a and 2b sites, corresponding to O3- and O2-domains, respectively.

Another important difference is found in the peak profile for the diffraction patterns in Figure 4. The peak profile of the O4-phase is much broader than those of O3- and O2-type $LiCoO_2$ polymorphs and the OP4-type precursor. As compared in Figure S2 (Supporting Information), although the peak positions of the O4-phase exactly match those of the simulated pattern, a clear difference is noted in the peak profile. The peak profile broadening is also evident in the TOFND pattern in Figure 4b. The fwhm of the 110 diffraction line for the TOFND pattern of the O4 phase is found to be fairly narrow, which is almost the same before and after ion-exchange. In contrast, the peak profile broadening was observed for 10l lines. Because the (110) plane is aligned perpendicularly to the CoO_2 layers, its fwhm is highly influenced by the in-plane crystallinity of the layers. The narrow fwhm of the 110 line for the O4-phase found by high-resolution ND suggests that the CoO_2 layers were not damaged and/or strained by the ion-exchange process. The peak profile broadening originates from the gliding of the CoO_2 layers associated with stacking faults that are further discussed in the next section.

Stacking Faults for O4-type $LiCoO_2$. SEM observation clearly reveals that the Na/Li ion-exchange results in the stacking faults as shown in Figure 5. The as-prepared OP4-phase crystallizes into a smooth, faceted hexagonal plate-like morphology with the size more than 10 μm. The smooth facets are lost after ion-exchange; instead, many steps appear on the particles of the O4-phase. Electron diffraction measurements also support the presence of through-plane stacking faults in the O4-phase (see Figure S3, Supporting Information). It is noted that the particle morphology of the O4-phase is clearly different than that in the previous report for the O2-type phase.[19] The stepped facets found for the O4-phase were not observed in the O2-phase, which is consistent with the fact that the stacking fault was not evidenced for the O2-type phase, because the formation of nucleation centers is dominated by the growth of O2-domains.[32] Although O2 and O4 phases are similarly prepared by ion-exchange, the frequency of stacking faults induced is clearly significant for the O4-phase, suggesting that the growth of the O4-domains is dominated by its nucleation process. The difference probably originates from the existence of CoO_2−Li−CoO_2 blocks as O3-domains in the OP4-phase. Through-plane Na−Na interaction via CoO_6 octahedra could be disturbed by the presence of CoO_2−Li−CoO_2 blocks. Therefore, the growth process of the O4-phase is dominated by the nucleation process for ion-exchange in the OP4-phase, leading to the formation of stacking faults. Several different experimental conditions have been utilized for ion-exchange to reduce the nucleation rate (and less stacking faults). However, a similar amount of the stacking faults deduced from XRD patterns was always found regardless of the experimental conditions, or ion-exchange was not completed.

The stacking faults in the O4-phase were further analyzed by using the DIFFaX program.[26] Figure 6 compares schematic illustrations of potential phases formed after ion-exchange, O4 (O4′)-, O8-, and O12-phases. In this study, intergrowth models consisting of these phases were utilized. A model with OP4/O4 intergrowth was not considered because Na ion contents found in the O4-phase were negligible. In Figure 6, the CoO_2−Li−CoO_2 blocks are numbered from 1 to 6 for the OP4-phase. Ideally, the blocks with odd numbers, 1, 3, and 5, do not move

Table 3. Comparison of Crystallographic Parameters for Three Different $LiCoO_2$ Polymorphs. Crystallographic Parameters of OP4-$Li_{0.37}Na_{0.31}CoO_2$ Are Also Shown for Comparison

	O3-$LiCoO_2$ (ref 4)	O2-$LiCoO_2$ (ref 16)	O4−$Li_{0.9}CoO_2$ (this study)	OP4-$Li_{0.37}Na_{0.31}CoO_2$ (this study)
space group	$R\bar{3}m$	$P6_3mc$	$P6_3mc$	$P6_3/mmc$
a axis (Å)	2.817	2.802	2.813	2.821
c axis (Å)	14.06	9.536	18.86	20.28
interlayer distance (Å)	4.69	4.77	4.72 (average)	5.07 (average)

dx.doi.org/10.1021/ic4013922 | Inorg. Chem. 2013, 52, 9131−9142

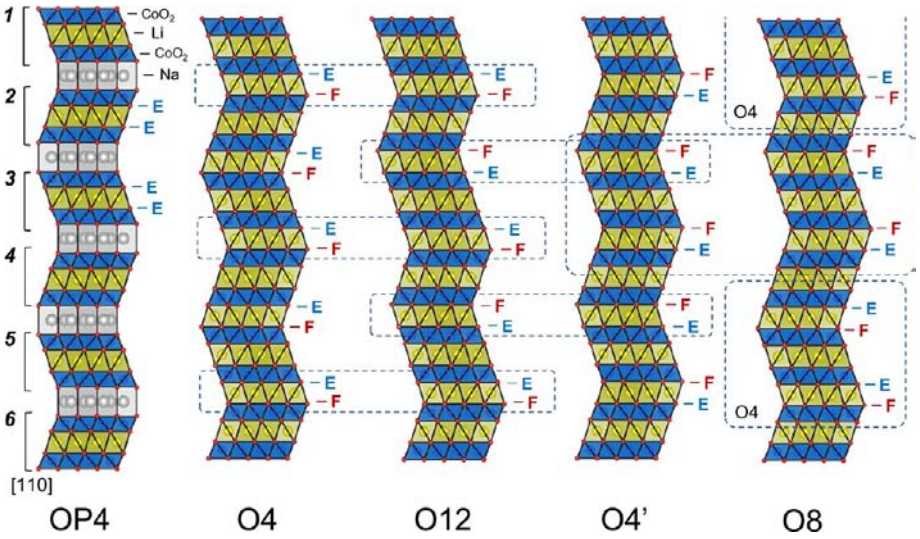

Figure 6. Schematic illustrations of crystal structures for the OP4-phase, and for O4-, O4′-, O8-, and O12-phases that are potentially prepared from the OP4-phase by Na/Li ion-exchange. "E" and "F" denote edge- and face-sharing planes of LiO_6–CoO_6, respectively. In contrast, for the O3-phase (or O3-domains), Li ions (LiO_6 octahedra) only share edges (denoted as "E") with CoO_6 octahedra. See the text for more details.

and the blocks stay at their original positions, whereas the blocks with even numbers, 2, 4, and 6, move toward the (2/3, 1/3, z) direction, forming the ideal O4-phase. Similar to this phase, when the even-numbered blocks glide toward the direction of (1/3, 2/3, z), the O4′-phase is formed, as shown in Figure 6. The difference between O4- and O4′- phases is the positions of the face- and edge-shared planes. Both phases are crystallographically identical to each other. When the O4′-phase is rotated by 180° (the rotation axis is perpendicular to the page and [110] for the OP4-phase), the O4′-phase is superimposed to the O4-phase. However, if some even-numbered blocks move randomly toward either translation vectors, (2/3, 1/3, z) or (1/3, 2/3, z), this gliding process induces the stacking faults in the structure, that is, a random O4/O4′ intergrowth structure. The influence of the random O4/O4′ intergrowth structure on the XRD peak profile is first simulated using the DIFFaX program. Crystallographic parameters of two distinct CoO_2–Li–CoO_2 blocks used for the simulation, which correspond to odd- and even-numbered blocks in Figure 6, respectively, are listed in Table S1 (Supporting Information). A simulated XRD pattern using the random O4/O4′ intergrowth model is shown in Figure S4 (Supporting Information). Although the peak intensity and background profile are slightly influenced, as shown in Figure S4, peak broadening as observed for the experimentally prepared O4-phase is not reproduced with this model. Because the O4- and O4′-phases are crystallographically identical to each other, the random O4/O4′ intergrowth model only influences the peak intensity, and not the profile.

The second model utilized was an O8-phase. The structural model of the O8-phase is also found in Figure 6. The O8-phase is also formed with 50% of the block gliding and highly correlated to the O4- and O4′-phases. For the O8-phase, odd-numbered blocks are immobilized, and even-numbered blocks alternately glide toward (2/3, 1/3, z) and (1/3, 2/3, z), for example, block 2 (2/3, 1/3, z), block 4 (1/3, 2/3, z), block 6 (2/3, 1/3, z), and so on. This type of gliding manner is classified as an "ordered" O4/O4′ intergrowth phase. A simulated XRD pattern of the O8-phase is found in Figure S5 (Supporting Information). Since the O8-phase is the superstructure between O4- and O4′-phases (see Figure 6), superlattice lines appear based on the fundamental diffraction lines of the O4(O4′) phase. However, these superlattice lines are not observed in the SXRD pattern of the O4-phase. Therefore, the possibility of O8-phase formation is eliminated. The odd-numbered blocks for the O4-, O4′-, and O8-phases were immobilized to their original positions without the gliding, because this restriction minimizes a number of the gliding layers (50%) by ion-exchange. Although the phase formation of O4-, O4′-, and O8-phases presumably affects the stacking sequences, experimental peak broadening observed for the SXRD and ND patterns in Figures 3 and 4 cannot be reproduced with these models of stacking faults.

Therefore, we have utilized the third model, that is, an O12-phase. The number of gliding layers increases to 66.7% in the O12-model. Two out of three CoO_2–Li–CoO_2 blocks move by ion-exchange. An ideal sequence for the gliding is described as follows: blocks 1 and 4 stay at their original positions, blocks 2 and 5 move toward (2/3, 1/3, z), and blocks 3 and 6 move toward (1/3, 2/3, z), resulting in the formation of the O12-phase, as shown in Figure 6. The O12-phase is also considered to be an ordered intergrowth structure of O4/O4′-phases, as shown in Figure 6, even though the fraction of gliding layers increases to 66.7%. The sequence of face- and edge-shared sites alternately changes along the c-axis direction in the O12-phase. A simulated XRD pattern of the O12-phase is shown in Figure 7. The XRD pattern of the O12-phase is completely different from that of the O4(O4′)-phase, except for the (110) and (00l) lines. Therefore, the change in the XRD pattern profile is expected by assuming the formation of an intergrowth model between O4/O12-phases. Note that the O4/O12 intergrowth model used in this study is essentially an analogue model with the O2/O6 intergrowth model proposed by Lu and Dahn,[33] except that MeO_2 layers are extended to the MeO_2–Li–MeO_2 blocks as gliding layers. Simulated XRD patterns of the intergrown O4/O12 phase with different probabilities are also shown in Figure 7. In this simulation, O12-domains are randomly inserted based on the ideal O4-phase model shown in Table 2. As shown in Figure 7, the peak profile is drastically broadened with the increase in the probability of stacking faults,

dx.doi.org/10.1021/ic4013922 | Inorg. Chem. 2013, 52, 9131–9142

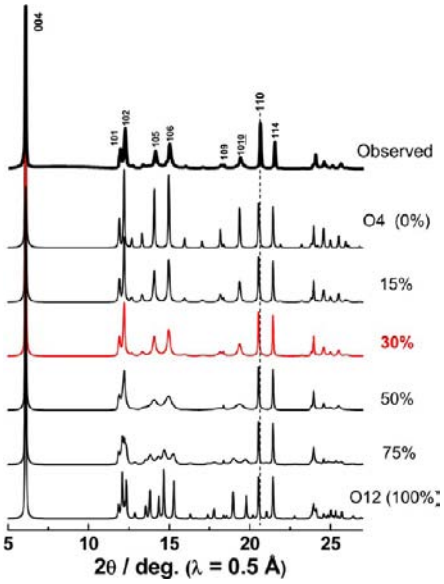

Figure 7. Simulated SXRD patterns of O4/O12 intergrowth phases using the DIFFaX program. The observed SXRD pattern of the O4-phase is also shown for comparison. Peak broadening observed for the O4-phase is nicely reproduced by assuming the presence of stacking faults with approximately 30% O12-domains.

except for the (110) and (00*l*) lines. The maximum broadening is observed for the 1:1 random intergrowth structure (50%) between O4- and O12-phases, and this phase also corresponds to the layered structure with the complete random sequence for the stacking of CoO_2−Li−CoO_2 blocks (each block glides toward either (1/3, 2/3, *z*) or (2/3, 1/3, *z*) without any restrictions). From the simulated XRD patterns shown in Figure 7, approximately 30% of O12-domains are expected to exist in the experimentally prepared O4-phase. It is also clear that the O12-phase is not the major phase, because no experimental evidence is found for the intrinsic lines from the O12-phase. As discussed above, the through-plane interaction among Na layers could be weak in the OP4-phase. Therefore, ion-exchange (the formation of nucleation centers) and block gliding start throughout the crystallite particles in the OP4-sample, resulting in the almost random through-plane stacking of the blocks, that is, random intergrowth structures of O4, O4′, O12, and other possible phases. The domains based on the random O4/O4′ intergrowth structure also must exist in this sample. Because this type of intergrowth does not much affect the peak profile of the sample (Figure S4, Supporting Information), the formation of these domains contributes to maintaining a sharp peak profile. Thus, it is reasonable to conclude that the experimentally prepared O4-$LiCoO_2$ by the hydrothermal ion-exchange contains roughly 30% of O12-domains after ion-exchange, as shown in Figure 7.

X-ray Absorption Spectroscopy. Local and electronic structures of cobalt for three $LiCoO_2$ polymorphs were examined by X-ray absorption spectroscopy (XAS). Figure 8 shows X-ray absorption near-edge structure (XANES) spectra of $LiCoO_2$ polymorphs at the Co K-edge. Extended X-ray absorption fine structure (EXAFS) spectra and refined parameters are also compared in Figure S6 and Table S2 (Supporting Information), respectively. From the EXAFS spectra, the difference among the polymorphs is negligible at least for the first and second coordination shells, which correspond to Co-O and Co-Co shells, respectively. The major

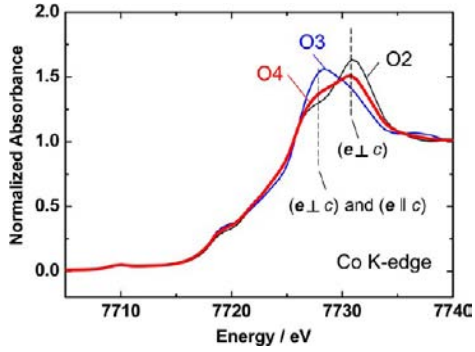

Figure 8. XANES spectra at Co K-edge for three $LiCoO_2$ polymorphs.

difference must be found in the location of Li for these polymorphs from the structural point of view. Photoelectrons ejected from Co by X-ray absorption are scattered by electron clouds of surrounding atoms, resulting in the oscillations observed in the XAS spectra. However, such ejected photoelectrons are not significantly scattered by Li ions. Therefore, it is difficult to distinguish these $LiCoO_2$ polymorphs from EAXFS spectra.

In contrast to EXAFS, a clear difference is found in XANES spectra, as shown in Figure 8. As discussed in the previous section, although the experimentally prepared O4-type $LiCoO_2$ has a significant amount of stacking faults, the local structure near cobalt ions should not be influenced by the formation of stacking faults with O12-domains. Half of the CoO_6 octahedra are only edge-shared with LiO_6 octahedra (O3-domains), and the rest of the CoO_6 octahedra are edge- and face-shared with lithium (O2-domains). Recently, Koyama et al. theoretically predicted the difference in the XANES spectra of $LiCoO_2$ polymorphs by DFT calculations.[34] Because the $LiCoO_2$ polymorphs have a character as the layered materials, the electric dipole transition probability from the 1s core level at the Co K-edge depends on the polarization direction of the X-ray; the direction of the electric field ***e*** to the *c* axis of $LiCoO_2$ is either parallel (***e*** ∥ *c*) or perpendicular (***e*** ⊥ *c*). According to the literature,[34] the absorption peak at 7728 eV could be contributed by both (***e*** ∥ *c*) and (***e*** ⊥ *c*) transitions, whereas the peak at 7731 eV could be mainly contributed by the (***e*** ⊥ *c*) transition. For the O3-$LiCoO_2$, the transition probability that originates from the (***e*** ∥ *c*) transition clearly increases in comparison to that for O2-$LiCoO_2$. Therefore, the absorption intensity at 7728 eV increases for the O3-phase, as shown in Figure 8. Since the O4-$LiCoO_2$ is the intergrowth structure between O3- and O2-$LiCoO_2$, a spectrum of the O4-phase lies in between the O2- and O3-phases. The result is consistent with the structural analysis in the previous section, and thus it is concluded that XANES spectra are useful to analyze and distinguish the detailed structures even for layered polymorphs at the specific element existing in similar environments.

Electrochemical Behavior of $LiCoO_2$ Polymorphs as the Electrode Materials. In this section, electrochemical properties of three $LiCoO_2$ polymorphs in Li cells are compared. Figure 9a shows galvanostatic oxidation/reduction curves of Li cells, and those differential d*x*/d*V* plots are also compared in Figure 9b. When the Li cells are charged to 4.8 V, almost all of the lithium ions are extracted from O3-type $LiCoO_2$. Approximately 80% of Li ions are reinserted into the O3-phase. The reversible capacity observed at a rate of 20 mA g^{-1} is the highest (~220 mAh g^{-1} of reversible capacity) among

dx.doi.org/10.1021/ic4013922 | Inorg. Chem. 2013, 52, 9131−9142

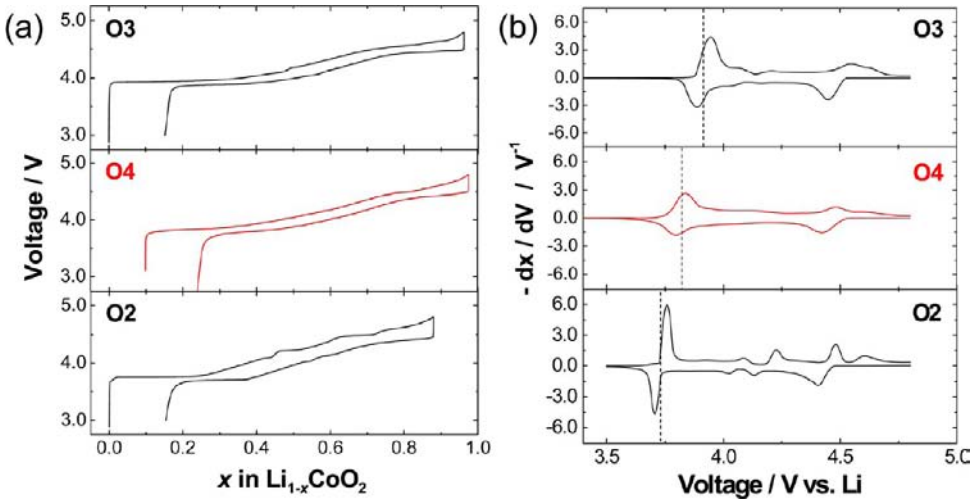

Figure 9. (a) Galvanostatic oxidation/reduction curves of Li cells with different $LiCoO_2$ polymorphs, and (b) those differential dx/dV plots. Dotted lines are guides for the eyes.

the three polymorphs. In the differential capacity plots, two voltage peaks centered at approximately 3.9 and 4.5 V are observed with an additional two small peaks at around 4.15 V ($x \approx 0.5$ in Li_xCoO_2). The appearance of these small peaks is associated with a monoclinic phase transition because of the Li/vacancy ordering in $Li_{0.5}CoO_2$.[5,9] This monoclinic phase is denoted as the O′3-phase with distorted octahedral sites. For the O2-phase, several sets of voltage plateaus that originate from the complicated phase transitions associated with the gliding of CoO_2 layers are observed.[17,18,35] In contrast to the O2-phase, clear phase transitions are not evidenced for the O4-phase at least from the electrochemical data in Figure 9, which will be further discussed in the next section. A clear difference is found in oxidation/reduction processes with the lowest voltage region (see dotted lines in Figure 9b) for each sample. The voltage in this region is approximately 0.17 V lower for the O2-phase: 3.73 V for O2 vs 3.90 V for O3. The voltage of the O4-phase lies in between that of O2 and O3. Note that, for the O4-phase, Li ions are located at two different sites: 2a sites (face- and edge-shared sites, similar to O2) and 2b sites (edge-shared sites, similar to O3), as shown in Table 2. Although it is still unknown whether Li ions are extracted selectively or simultaneously from 2a and 2b sites, it is hypothesized that Li ions are simultaneously extracted from both sites. Therefore, the O4-phase shows the intermediate voltage between O2- and O3-phases in this region. Further study is needed to test this hypothesis. In the literature, rate capability and cyclability of the O2-phase as electrode materials in Li cells are reported to be similar to those of the O3-phase.[18] The O4-phase also shows competitive rate capability and cyclability with the O3-phase.[22]

Structural Phase Transitions for O4-$LiCoO_2$. Since the difference is expected in the reversible phase transition behavior from the electrochemical properties in Figure 9, in this section, structural phase transitions of the O4-phase are examined and compared with the O2- and O3-phases. SXRD was employed to study the change in crystal structures during Li-extraction processes for the O4-phase. Figure 10 shows SXRD patterns of $Li_{0.9-x}CoO_2$ ($0 \le x \le 0.8$). Highlighted SXRD patterns are also shown in Figure 11. Important findings are summarized as follows. For $0 \le x < 0.2$, O4-$Li_{0.9-x}CoO_2$ exists as a single phase. For $x = 0.2$, the peak profile becomes broad, and two layered phases are found to coexist, as is clearly observed in the

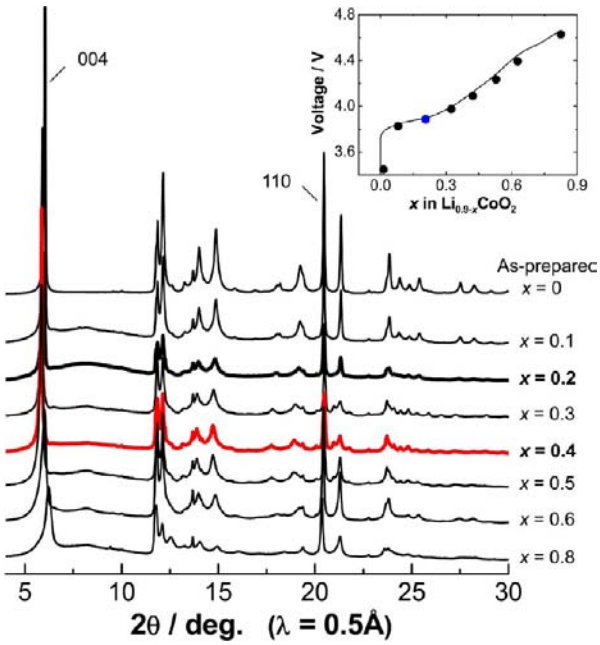

Figure 10. SXRD patterns of O4-$Li_{0.9-x}CoO_2$ ($0 \le x \le 0.8$). The points where SXRD data were collected are shown in the inset.

highlighted pattern in Figure 11a. The second phase exists as a single phase for $0.3 \le x \le 0.5$. As shown in Figure 11a, the 004 diffraction line discontinuously shifts to a lower diffraction angle (for $0.1 < x < 0.3$), which is indicative of a first-order phase transition. Interlayer distances calculated from the position of 004 diffraction lines are plotted in Figure 12, in which the data of the O3-phase[7] and O2-phase[35] are also plotted for comparison. Lattice parameters discontinuously increase with the appearance of this second phase (approximately 0.06 Å gap). Although the peak profile is broad because of stacking faults, two new peaks appear on the diffraction patterns at 21.0 and 21.8°, as shown in Figure 11b. These peaks cannot be indexed using the O4-phase. Instead, the diffraction lines can be indexed using a model of OT#4-type $Li_{1-x}CoO_2$, that is, an intergrowth structure between O3- and T#2-phases in our previous paper,[22] where it is denoted as the OT4-phase. The formation of the T#2-phase has been reported for the O2-

dx.doi.org/10.1021/ic4013922 | Inorg. Chem. 2013, 52, 9131−9142

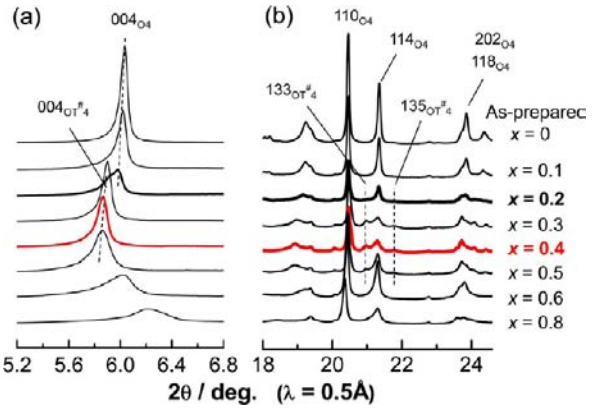

Figure 11. Highlighted SXRD patterns of O4-$Li_{0.9-x}CoO_2$ ($0 \leq x \leq 0.8$) shown in Figure 10. Two-phase coexistence is observed at x = ~0.2, and then the second phase is isolated as the $OT^{\#}4$-phase at $0.3 \leq x \leq 0.6$.

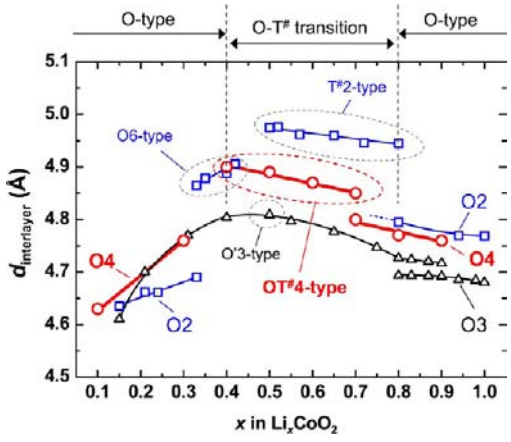

Figure 12. Comparison of changes in interlayer distances for three $LiCoO_2$ polymorphs. Three $LiCoO_2$(s) show different characters as polymorphs consisting of CoO_2 layers. See the text for more details.

$Li_{1-x}CoO$ upon Li extraction to x = ~0.5,[35] after the report on T2-$Li_{2/3}[Ni_{1/3}Mn_{2/3}]O_2$.[36] The formation of the $T^{\#}2$-phase is achieved by the gliding of CoO_2 layers toward the direction of (1/3, 1/6, z) based on the O2-phase. Li ions are located at two different tetrahedral sites, 8e sites with four equal Li−O distances (see Figure 13) and 8f sites at distorted edge-shared tetrahedral sites with CoO_2 layers.[35] The O2-phase coexists with the $T^{\#}2$-phase in the range of $0.72 < x < 0.80$, and the $T^{\#}2$ single phase region was found for $0.5 \leq x \leq 0.72$. Because electrostatic repulsion between CoO_2 layers for the $T^{\#}2$-type stacking is larger than that for O2-type stacking, interlayer distances anomalously increase, as shown in Figure 12. An ideal model of the $OT^{\#}4$-$Li_{0.5}CoO_2$ phase is shown in Table 4. Note

Table 4. Crystallographic Parameters of $OT^{\#}4$-$Li_{0.5}CoO_2$[a]

$OT^{\#}4$-$Li_{0.5}CoO_2$[b]					
atom	site	g	x	y	z
Co	8f	1.00	0	1/3	0.619
Li (1)	4b	0.50	1/2	0	0
Li (2)	8e	0.20	1/4	1/4	1/4
Li (3)	8f	0.05	0	1/3	0.258
O (1)	8f	1.00	0	5/6	0.066
O (2)	8f	1.00	0	0	0.328

[a]These parameters, except lattice parameters, were not refined because of the presence of stacking faults. [b] S.G.: *Cmca*. a = 2.80 Å, b = 4.85 Å, and c = 19.46 Å.

that the Rietveld analysis was not conducted because of the existence of numerous stacking faults. According to the literature,[37] Li ions are hypothetically located at both 8e and 8f tetrahedral sites for $T^{\#}2$-domains and at edge-shared octahedral sites for O3-domains in Table 4. Observed and simulated XRD patterns are compared in Figure S7 (Supporting Information). The additional two diffraction lines are nicely assigned into (133) and (135) lines of the $OT^{\#}4$-phase. In addition, the interlayer distances of O4($OT^{\#}4$)-phases lie in between O3(O′3)- and O2($T^{\#}2$)-phases, which

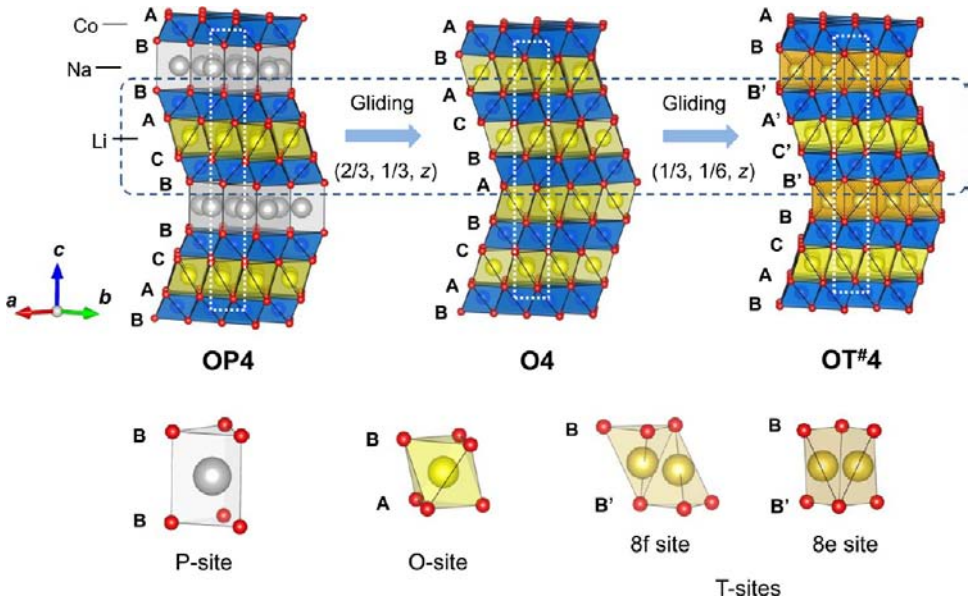

Figure 13. Schematic illustrations of phase transition behavior for the OP4-, O4-, and $OT^{\#}4$-phases. Tetrahedral sites for the $OT^{\#}4$-phase are expected to be the same for the $T^{\#}2$-type $Li_{0.5}CoO_2$ that are obtained from the O2-type phase.

dx.doi.org/10.1021/ic4013922 | *Inorg. Chem.* 2013, 52, 9131−9142

are also consistent with the intergrowth model. From these facts, it is concluded that the O4-phase is translated into the OT#4-phase during lithium extraction, and this finding is the first report of the intergrowth structure between O3- and T#2-phases. Similar to the O2-phase, the formation of the OT#4-phase is achieved by gliding of CoO_2−Li_x−CoO_2 blocks with O3-domains toward the direction of (1/3, 1/6, z) based on the O4-phase, as shown in Figure 13.

Further oxidation beyond $x > 0.5$ in O4-$Li_{1-x}CoO_2$ results in the shrinkage of interlayer distances. In this region, for the O2-system, O6-$Li_{1-x}CoO_2$ ($0.5 < x < 0.67$) appears as a result of an additional phase transition.[17,18,35] For the O4-system, no clear evidence for O12-phase formation is found, which is the intergrowth structure between O3- and O6-phases, as shown in Figure 6. Interlayer distance clearly decreases upon charge beyond $x \geq 0.6$ in O4-$Li_{1-x}CoO_2$, and observed XRD patterns can be assigned into the O4-phase. The phase transition processes during Li extraction for the O4-phase are somewhat suppressed compared with the O2-phase. The difference can be explained by the presence of the stacking faults in the O4-phase. Ideally, OT#4-phase formation from the O4-phase is achieved by the gliding of 50% of CoO_2−Li−CoO_2 blocks. Additionally, the T#-phase can be formed in not only O4- but also O12-phases with 50% gliding of the blocks. The formation of the OT#4-phase, therefore, was not influenced by the stacking fault with 30% of O12-domains. In contrast to the T#-phase, O12-phase formation is influenced by the presence of stacking faults. The sample already has 30% O12-domains, which are "randomly" distributed in the particles. To form the O12-phase with less stacking faults, regliding and reconstruction for stacking sequences are required for a large part of the CoO_2−Li−CoO_2 blocks (note that at least 12 CoO_2 layers, or 6 CoO_2−Li−CoO_2 blocks, are needed to stack properly to form the O12-phase, as shown in Figure 6). This process is expected to be energetically unfavorable, and therefore, the O12-phase was not observed in the O4-phase.

When 80−90% of Li ions are extracted from three $LiCoO_2$ polymorphs, similar interlayer distances are observed (4.60−4.62 Å). Since the Li ions at face-shared sites with CoO_6 octahedra increase the interlayer distance for the O2-phase with large repulsive interaction, the observed interlayer distance is consistent with this fact. Less repulsive interaction is expected after Li removal. Although peak broadening and shortened interlayer distance are found in Figures 10−12 by oxidation to $x = 0.8$ in O4-$Li_{1-x}CoO_2$, the peak profile becomes sharp by reinsertion of lithium. The reversibility is found to be high enough, and the bulk crystal structure is not damaged.

An additional phase transition,[7] formation of the T1[15]-phase (instead of T1, "O1" is often used in the literature), is observed for the O3-phase by the translation of the CoO_2 layer toward the (1/3, 2/3, z) direction after nearly complete Li extraction. Such phase transition is not observed for the O2-phase because gliding of CoO_2 layers toward (1/3, 2/3, z), or (2/3, 1/3, z) results in only exchange in the positions of face- and edge-shared sites with CoO_2 layers, similar to the relation between O4- and O4′-phases, as discussed in the former section (Figure 6). As the O4-phase also has the O3-domains, the formation of an intergrowth phase between T1- and O2-phases is expected after the complete Li extraction. This process may not be influenced by the stacking faults because the T1-phase formation is accomplished in O3-domains. However, it has not succeeded in isolation of this intergrowth phase, presumably because of kinetic limitations for Li extraction from the O3-domains.

CONCLUSIONS

A single phase of OP4-[Li, Na]CoO_2 was synthesized and used as a precursor to prepare the third polymorph of $LiCoO_2$ by ion-exchange. This polymorph consists of ideally four CoO_2 layers to describe a unit cell, and Li ions are located at two octahedral sites with different environments. According to the classification proposed by Delmas, the structure is classified as O4-type $LiCoO_2$, which is an intergrowth phase of O2- and O3-type $LiCoO_2$. Three polymorphs are composed of two-dimensional CoO_2 layers, and those polymorphs possess the different types of close-packed oxygen packing. Although the peak profile of O4-type $LiCoO_2$ is broad for 10l diffraction lines, the peak width broadening for the 110 diffraction line is not observed even by the high-resolution neutron diffraction. This fact indicates that the peak broadening originates from the presence of stacking faults, and CoO_2 layers are not damaged by ion-exchange. Structural analysis with the DIFFaX program suggests that O12-domains (∼30%) are randomly inserted based on the ideal O4-phase. The fact also suggests that gliding of layers nearly randomly occurs toward either the (2/3, 1/3, 0) or the (1/3, 2/3, 0) direction. For OP4-[Li, Na]CoO_2, Na layers with prismatic sites are sandwiched between the O3-$LiCoO_2$ domains. Crystal growth of O4-domains during ion-exchange is expected to be disturbed by the existence of O3-domains. Thus, a considerable amount of nucleation centers is created by ion-exchange, resulting in the stacking faults. Although stacking faults exist, this phase is classified as the intergrowth phase of O2- and O3-phases, as supported by XAS spectroscopy. The stacking faults in the sample seem to influence the electrochemical properties and phase transition behavior. For the O2-type $LiCoO_2$, the original O2-phase reversibly transforms into T#2- and O6-phases. In contrast, for the O4-phase, the formation of the O12-phase as an intergrowth phase of O3/O6 is not confirmed, whereas the OT#4-phase is isolated as OT#4-$Li_{0.5}CoO_2$. The T#-domains can be formed from both O4- and O12-domains with the minimum amount (50%) of CoO_2−Li−CoO_2 block gliding, whereas the O12-phase formation requires the considerable reconstruction process. The results are also consistent with electrochemical measurements; voltage plateaus with two-phase regions are less evident for the O4-phase in comparison to the O2-phase. For layered materials, such as $LiCoO_2$[11,38] and $LiNiO_2$,[39,40] the formation of point defects, such as antisite defects and off-stoichiometry, impurity, oxygen vacancy, etc., is often discussed as important factors affecting the boundaries of solid−solid two-phase miscibility. Similar to the point defects, it is concluded that stacking faults as a planar defect could also influence such phase transition behavior for layered materials.

ASSOCIATED CONTENT

Supporting Information

Tables containing crystallographic parameters and a summary of the analysis of Co K-edge EXAFS spectra and figures showing a result of the Rietveld refinement for OP4-$Li_{0.37}Na_{0.31}CoO_2$, SXRD patterns, electron diffraction patterns, simulated XRD patterns, radial distribution of the cobalt ions, and XRD patterns. This material is available free of charge via the Internet at http://pubs.acs.org.

dx.doi.org/10.1021/ic4013922 | Inorg. Chem. 2013, 52, 9131−9142

AUTHOR INFORMATION

Corresponding Author

*E-mail: komaba@rs.kagu.tus.ac.jp.

Notes

The authors declare no competing financial interest.

ACKNOWLEDGMENTS

This study was, in part, granted by JSPS through the "Funding for NEXT Program," and MEXT program "Elements Strategy Initiative to Form Core Research Center" (since 2012), MEXT, Ministry of Education Culture, Sports, Science and Technology, Japan. The SXRD experiments were made possible through the support of the Japanese Ministry of Education, Science, Sports and Culture, the Nanotechnology Support Project (Proposal No. 2011B1729 and 2012A1672), with the approval of the Japan Synchrotron Radiation Research Institute (JASRI). The neutron scattering experiment was approved by the Neutron Science Proposal Review Committee of J-PARC/MLF (Proposal Nos. 2009B0016 and 2010B0024) and supported by the Inter-University Research Program on Neutron Scattering of IMSS, KEK. The synchrotron X-ray absorption work was done under the approval of the Photon Factory Program Advisory Committee (Proposal No. 2011G141). N.Y. gratefully acknowledges financial support by Grant-in-Aid for Young Scientists (B) (No. 24750186) from MEXT. We also acknowledge experimental support for TEM/ED by Nissan Arc Ltd.

REFERENCES

(1) Whittingham, M. S. *Science* **1976**, *192*, 1126−1127.
(2) Dampier, F. W. *J. Electrochem. Soc.* **1974**, *121*, 656−660.
(3) Whittingham, M. S. *J. Electrochem. Soc.* **1975**, *122*, 713−714.
(4) Mizushima, K.; Jones, P. C.; Wiseman, P. J.; Goodenough, J. B. *Mater. Res. Bull.* **1980**, *15*, 783−789.
(5) Reimers, J. N.; Dahn, J. R. *J. Electrochem. Soc.* **1992**, *139*, 2091−2097.
(6) Ohzuku, T.; Ueda, A. *J. Electrochem. Soc.* **1994**, *141*, 2972−2977.
(7) Amatucci, G. G.; Tarascon, J. M.; Klein, L. C. *J. Electrochem. Soc.* **1996**, *143*, 1114−1123.
(8) Menetrier, M.; Saadoune, I.; Levasseur, S.; Delmas, C. *J. Mater. Chem.* **1999**, *9*, 1135−1140.
(9) Shao-Horn, Y.; Levasseur, S.; Weill, F.; Delmas, C. *J. Electrochem. Soc.* **2003**, *150*, A366−A373.
(10) Shao-Horn, Y.; Croguennec, L.; Delmas, C.; Nelson, E. C.; O'Keefe, M. A. *Nat. Mater.* **2003**, *2*, 464−467.
(11) Menetrier, M.; Carlier, D.; Blangero, M.; Delmas, C. *Electrochem. Solid-State Lett.* **2008**, *11*, A179−A182.
(12) Lu, Y.-C.; Mansour, A. N.; Yabuuchi, N.; Shao-Horn, Y. *Chem. Mater.* **2009**, *21*, 4408−4424.
(13) Shannon, R. D. *Acta Crystallogr., Sect. A* **1976**, *32*, 751−767.
(14) Mather, G. C.; Dussarrat, C.; Etourneau, J.; West, A. R. *J. Mater. Chem.* **2000**, *10*, 2219−2230.
(15) Delmas, C.; Fouassier, C.; Hagenmuller, P. *Physica B+C* **1980**, *99*, 81−85.
(16) Delmas, C.; Braconnier, J.-J.; Hagenmuller, P. *Mater. Res. Bull.* **1982**, *17*, 117−123.
(17) Mendiboure, A.; Delmas, C.; Hagenmuller, P. *Mater. Res. Bull.* **1984**, *19*, 1383−1392.
(18) Paulsen, J. M.; Mueller-Neuhaus, J. R.; Dahn, J. R. *J. Electrochem. Soc.* **2000**, *147*, 508−516.
(19) Carlier, D.; Saadoune, I.; Croguennec, L.; Ménétrier, M.; Suard, E.; Delmas, C. *Solid State Ionics* **2001**, *144*, 263−276.
(20) Balsys, R. J.; Davis, R. L. *Solid State Ionics* **1994**, *69*, 69−74.
(21) Berthelot, R.; Pollet, M.; Carlier, D.; Delmas, C. *Inorg. Chem.* **2011**, *50*, 2420−2430.
(22) Komaba, S.; Yabuuchi, N.; Kawamoto, Y. *Chem. Lett.* **2009**, *38*, 954−955.
(23) Berthelot, R.; Carlier, D.; Pollet, M.; Doumerc, J.-P.; Delmas, C. *Electrochem. Solid-State Lett.* **2009**, *12*, A207−A210.
(24) Nishibori, E.; Takata, M.; Kato, K.; Sakata, M.; Kubota, Y.; Aoyagi, S.; Kuroiwa, Y.; Yamakata, M.; Ikeda, N. *Nucl. Instrum. Methods Phys. Res., Sect. A* **2001**, *467*, 1045−1048.
(25) Izumi, F.; Momma, K. *Solid State Phenom.* **2007**, *130*, 15−20.
(26) Treacy, M. M. J.; Newsam, J. M.; Deem, M. W. *Proc. R. Soc. London, Ser. A* **1991**, *433*, 499−520.
(27) Ishigaki, T.; Hoshikawa, A.; Yonemura, M.; Morishima, T.; Kamiyama, T.; Oishi, R.; Aizawa, K.; Sakuma, T.; Tomota, Y.; Arai, M.; Hayashi, M.; Ebata, K.; Takano, Y.; Komatsuzaki, K.; Asano, H.; Takano, Y.; Kasao, T. *Nucl. Instrum. Methods Phys. Res., Sect. A* **2009**, *600*, 189−191.
(28) Newville, M. *J. Synchrotron Radiat.* **2001**, *8*, 322−324.
(29) Ren, Z.; Shen, J.; Jiang, S.; Chen, X.; Feng, C.; Xu, Z.; Cao, G. *J. Phys.: Condens. Matter* **2006**, *18*, L379−L384.
(30) Huang, Q.; Foo, M. L.; Pascal, R. A., Jr.; Lynn, J. W.; Toby, B. H.; He, T.; Zandbergen, H. W.; Cava, R. J. *Phys. Rev. B* **2004**, *70*, 184110.
(31) Carlier, D.; Cheng, J. H.; Berthelot, R.; Guignard, M.; Yoncheva, M.; Stoyanova, R.; Hwang, B. J.; Delmas, C. *Dalton Trans.* **2011**, *40*, 9306−9312.
(32) Tournadre, F.; Croguennec, L.; Saadoune, I.; Carlier, D.; Shao-Horn, Y.; Willmann, P.; Delmas, C. *J. Solid State Chem.* **2004**, *177*, 2790−2802.
(33) Lu, Z. H.; Dahn, J. R. *Chem. Mater.* **2001**, *13*, 2078−2083.
(34) Koyama, Y.; Arai, H.; Ogumi, Z.; Tanaka, I.; Uchimoto, Y. *Phys. Rev. B* **2012**, *85*, 075129.
(35) Carlier, D.; Saadoune, I.; Ménétrier, M.; Delmas, C. *J. Electrochem. Soc.* **2002**, *149*, A1310−A1320.
(36) Paulsen, J. M.; Donaberger, R. A.; Dahn, J. R. *Chem. Mater.* **2000**, *12*, 2257−2267.
(37) Tournadre, F.; Croguennec, L.; Saadoune, I.; Weill, F.; Shao-Horn, Y.; Willmann, P.; Delmas, C. *Chem. Mater.* **2004**, *16*, 1411−1417.
(38) Levasseur, S.; Menetrier, M.; Shao-Horn, Y.; Gautier, L.; Audemer, A.; Demazeau, G.; Largeteau, A.; Delmas, C. *Chem. Mater.* **2003**, *15*, 348−354.
(39) Rougier, A.; Gravereau, P.; Delmas, C. *J. Electrochem. Soc.* **1996**, *143*, 1168−1175.
(40) Croguennec, L.; Pouillerie, C.; Mansour, A. N.; Delmas, C. *J. Mater. Chem.* **2001**, *11*, 131−141.